Chemical Science

ROYAL SOCIETY OF CHEMISTRY

EDGE ARTICLE

View Article Online
View Journal | View Issue

Cite this: *Chem. Sci.*, 2024, **15**, 10477

All publication charges for this article have been paid for by the Royal Society of Chemistry

Received 26th March 2024
Accepted 31st May 2024

DOI: 10.1039/d4sc02002b

rsc.li/chemical-science

How does ferrocene correlate with ferroptosis? Multiple approaches to explore ferrocene-appended GPX4 inhibitors as anticancer agents†

Wei Li,‡[ab] Jing Yu,‡[ab] Jing Wang,‡[ab] Xuejing Fan,‡[ab] Ximing Xu,[c] Hui Wang,[ab] Ying Xiong,[d] Xinyu Li,[ab] Xiaomin Zhang,[ab] Qianer Zhang,[ab] Xin Qi,[ab] Pascal Pigeon,[ef] Qing Gu,[g] Julia Bruno-Colmenarez,[h] Gérard Jaouen,[ef] Michael J. McGlinchey,[h] Xue Qiu,[ab] Shu-Li You,[g] Jing Li*[ab] and Yong Wang*[ab]

Ferroptosis has emerged as a form of programmed cell death and exhibits remarkable promise for anticancer therapy. However, it is challenging to discover ferroptosis inducers with new chemotypes and high ferroptosis-inducing potency. Herein, we report a new series of ferrocenyl-appended GPX4 inhibitors rationally designed in a "one stone kills two birds" strategy. Ferroptosis selectivity assays, GPX4 inhibitory activity and CETSA experiments validated the inhibition of novel compounds on GPX4. In particular, the ROS-related bioactivity assays highlighted the ROS-inducing ability of **17** at the molecular level and their ferroptosis enhancement at the cellular level. These data confirmed the dual role of ferrocene as both the bioisostere motif maintaining the inhibition capacity of certain molecules with GPX4 and also as the ROS producer to enhance the vulnerability to ferroptosis of cancer cells, thereby attenuating tumor growth *in vivo*. This proof-of-concept study of ferrocenyl-appended ferroptosis inducers *via* rational design may not only advance the development of ferroptosis-based anticancer treatment, but also illuminate the multiple roles of the ferrocenyl component, thus opening the way to novel bioorganometallics for potential disease therapies.

Introduction

Ferroptosis was defined in 2012 as an iron-dependent form of programmed cell death caused by increased cellular reactive oxygen species (ROS) and lipid peroxidation (LPO).[1] Lipid metabolism, ROS biology, and iron regulation have been summarized as intersections from the centrality of the framework of ferroptosis.[2] In the past few decades, ferroptosis has been proven to engage in human diseases including cancer, neurodegeneration and ischemic disease.[3–9] Notably, accumulating evidence shows that ferroptosis plays important roles in cancer occurrence, development and metastasis, which highlights its great potential for the treatment of refractory tumors.[10] A deeper understanding of the epithelial–mesenchymal transition (EMT) in metastasis underscores the critical role of glutathione peroxidase 4 (GPX4) in cancer cells undergoing EMT; it is the only peroxidase in mammals capable of reducing lipid hydroperoxides.[11,12] Indeed, when GPX4 function is impaired, lipid peroxidation causes ferroptosis which is a tumor-suppressive process. Moreover, further research suggested that blocking GPX4 function or decreasing the protein level of GPX4 can suppress tumor growth.[13] Thus, aggressive neoplastic diseases might be treated through the use of GPX4 inhibitors.

Iron homeostasis composes the essential part of ferroptosis which is mainly mediated *via* the Fenton chain reaction.[14,15] Therefore, elevated levels of iron can increase the vulnerability to ferroptosis. The traditional Fenton system composed of H_2O_2 and Fe^{2+} has been intensively investigated and used in cancer treatment. The ferrocenyl group is perhaps the most widely studied organometallic moiety and enables the generation of

[a]*School of Medicine and Pharmacy, Key Laboratory of Marine Drugs, Chinese Ministry of Education, Ocean University of China, Qingdao 26003, Shandong, P. R. China. E-mail: lijing_ouc@ouc.edu.cn; wangyong8866@ouc.edu.cn*

[b]*Laboratory for Marine Drugs and Bioproducts, Pilot National Laboratory for Marine Science and Technology, Qingdao 266200, P. R. China*

[c]*Marine Biomedical Research Institute of Qingdao, School of Medicine and Pharmacy, Key Laboratory of Marine Drugs, Chinese Ministry of Education, Ocean University of China, Qingdao 266003, Shandong, P. R. China*

[d]*School of Pharmacy, Fudan University, Shanghai, 201203, China*

[e]*PSL, Chimie ParisTech, 11 Rue Pierre et Marie Curie, F-75005, Paris, France*

[f]*Sorbonne Université, UMR 8232 CNRS, IPCM, 4 Place Jussieu, F-75005, Paris, France*

[g]*State Key Laboratory of Organometallic Chemistry, Shanghai Institute of Organic Chemistry, Chinese Academy of Sciences, 345 Lingling Lu, Shanghai 200032, P. R. China*

[h]*UCD School of Chemistry, University College Dublin, Belfield, Dublin 4, Ireland*

† Electronic supplementary information (ESI) available: Experimental procedures for syntheses and biological evaluation, supplementary figures, schemes and tables, computational methods and details, cif files and X-ray data of **12**, **15** and **17**. CCDC 2310688–2310690. For ESI and crystallographic data in CIF or other electronic format see DOI: https://doi.org/10.1039/d4sc02002b

‡ These authors contributed equally.

ROS, which has contributed to its wide-spread exploration for use in medicinal chemistry.[16] The electron donor–acceptor ability of the central iron atom endows ferrocene with good redox characteristics and high catalytic capacity as an excellent Fenton catalyst, which effectively enhances the biological behavior of the original drugs.[17–20] Considering the high level of interest in ferroptosis, whose impetus towards the formation of lipid hydroperoxides arises from the iron-catalyzed Fenton reaction, exploration of the effect of ferrocene on the framework of ferroptosis (Fig. 1A) could be a valuable contribution. Thus far, however, comprehensive investigation of ferrocene in terms of ferroptosis inducers has been rather limited, and reported only for iron/ferrocene-based inorganic complexes or nanomaterials.[21–24]

In recent years, transition metal bioorganometallic chemistry has gradually come to the fore regarding its potential for the development of metallodrugs to circumvent the drawbacks[25–31] associated with platinum complexes.[32–37] Amongst the organometallic complexes that can be used as antitumoral agents, ferrocene occupies a privileged position as a compact, stable, non-toxic metallocene not only acting as a bioisostere for aryl/heteroaryl rings but also interfering in cellular redox homeostasis.[17,18,38–41] Initially, a library of ferrocene-based compounds (>100 entries) was established and then used to screen for ferroptosis inducers. Unfortunately, none of these random ferrocenyl-bearing entities could be characterized as ferroptosis inducers, although some have moderate cytotoxicities. These results indicated that regular ferrocenyl entities may not be able to induce ferroptosis significantly, which contradicted the conservative perception of ferrocene for ferroptosis and drove us towards the rational design of ferrocene-based ferroptosis inducers.

Thus, a "one stone kills two birds" strategy has been developed in this paper integrating the ferrocene fragment into typical ferroptosis inducers, such as the widely used GPX4 inhibitors (**ML162**, **RSL3** and **ML210**, Fig. 1B). We here describe multiple approaches towards the development of ferrocene-appended GPX4 inhibitors as anticancer agents, including structure-based drug design (SBDD), ferroptosis-targeted phenotypic evaluation and other molecular and cellular investigations. The ferroptosis selectivity assays, GPX4 inhibitory activity and CETSA experiments validated the inhibition of these novel compounds on GPX4. The ROS-related bioactivity assays emphasized the ROS-inducing ability of selected compounds at the molecular level and their ferroptosis enhancement at the cellular level. These data confirmed the dual role of ferrocene as both the bioisostere fragment maintaining the binding capacity of certain molecules with GPX4 and also as the ROS producer enhancing the vulnerability to ferroptosis of cancer cells, thereby attenuating tumor growth *in vivo*. This work describes a proof-of-concept study of ferrocene-appended dual-function ferroptosis inducers for cancer therapies *via* a rational design procedure, and consummated the potential application of ferrocene in ferroptosis-targeted drug development.

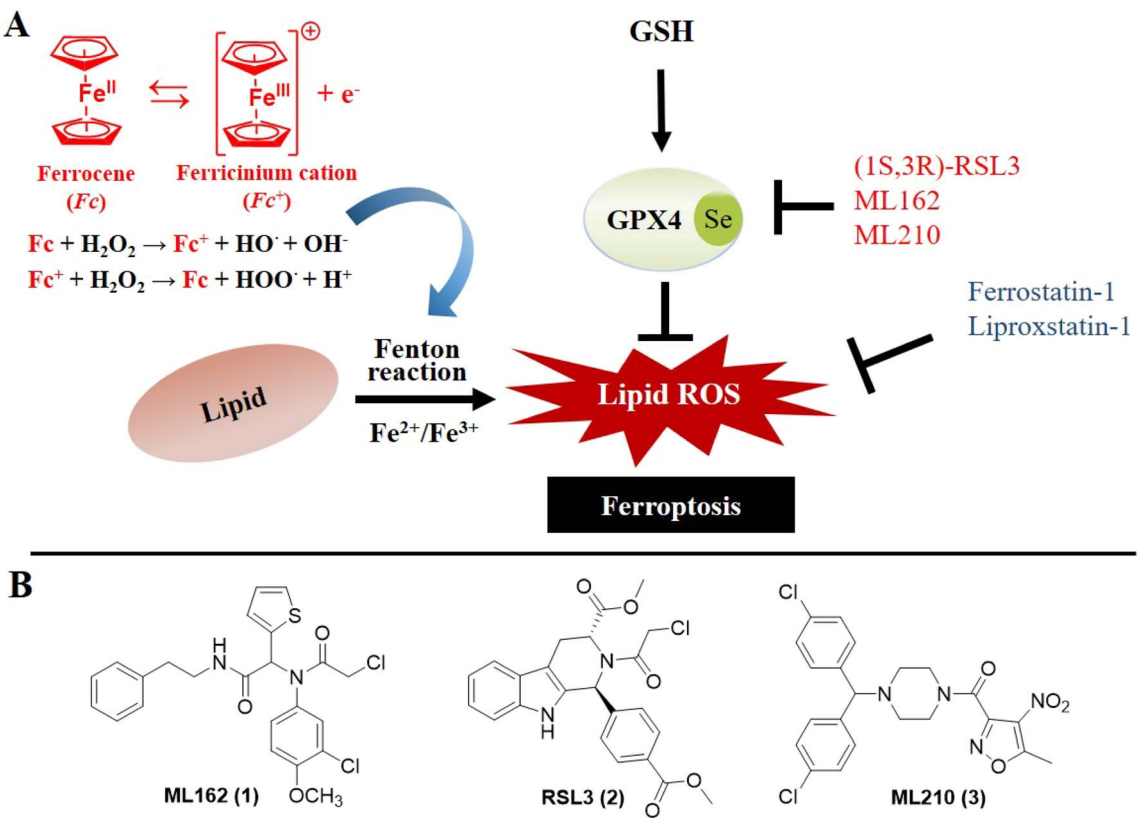

Fig. 1 (A) Illustration of the basis of developing ferrocene-based ferroptosis inducers. (B) Typical small molecule ferroptosis inducers.

Results and discussion

Ferrocene-based organometallic compound library construction and screening

The bioorganometallic community has explored the use of ferrocenyl compounds as inhibitors or as auxiliary groups to augment the efficacy of existing organic moieties, and some of them, such as ferroquine,[42] have entered clinical trials. In an initial approach to explore the potential of ferrocenyl compounds as ferroptosis inducers, an in-house ferrocene-based compound library was constructed, consisting of simple mono- or di-substituted ferrocenes, known ferrocene-based drug candidates such as the ferrocifen derivatives developed in our own laboratories,[43–46] aminoferrocene analogues from the Mokhir group[40,47] and ferroquine, as well as several chiral ferrocene derivatives reported by the You group[48–50] (Fig. 2A). Approximately 10% of the library was purchased from commercial sources and used without further modification, while the majority of the remaining complexes were either generous gifts from the original laboratory, or were prepared according to literature procedures. Initially, a primary screening was carried out for ferrocene complexes at two concentrations (1 and 10 μM) on ferroptosis-sensitive HT1080 cells, with or without ferrostatin-1 (fer-1), a known specific ferroptosis inhibitor.[1] For the complexes having moderate antiproliferative activities, their IC_{50} values were further tested to double check their ferroptosis selectivity. Unfortunately, although some of these organometallics can inhibit proliferation of HT1080 cells at the micromolar level, these cytotoxicities cannot be reversed significantly by the ferroptosis inhibitor fer-1, as shown in Fig. S1.† These results indicated that the antiproliferative effect of the tested ferrocene complexes may not be relevant to ferroptosis, even though some molecules have been claimed to produce ROS significantly at both the molecular and cellular levels including ferrocifen and amino-ferrocene derivatives.[40,51] These observations suggested there is no

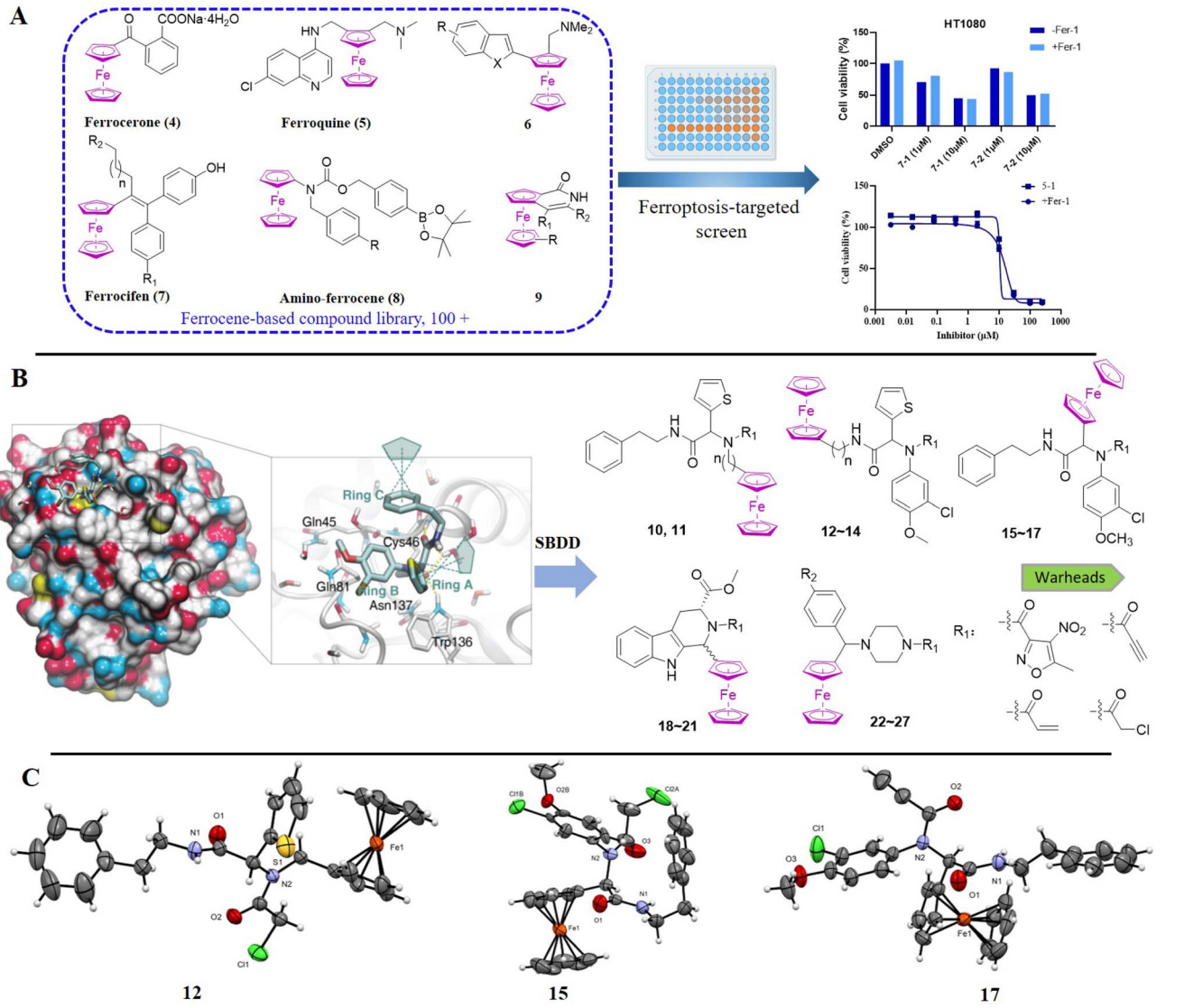

Fig. 2 (A) Illustration of the ferrocene-based organometallic compound library construction and screening. (B) Structure-based drug design (SBDD) of ferrocene-appended GPX4 inhibitors. (C) Molecular structures of the ferrocene complexes **12**, **15** and **17** with thermal ellipsoids shown at 50% probability.

immediate connection between ferrocene and ferroptosis, which highlights its unique mechanism.

Rational design and synthesis of ferrocene-appended GPX4 inhibitors

Apparently, the currently available ferrocene-based chemical entities could not induce ferroptosis, which prompted us to explore the effect of ferrocene in terms of ferroptosis *via* a rational design strategy. Inhibition of GPX4 with small molecules has been established as a pharmacological stimulator of ferroptosis, which can achieve durable responses in a range of cancer types supported by evidence both *in vitro* and *in vivo*.[52,53] The most well-known and potent GPX4 inhibitors involve two covalent binders **RSL3** and **ML162** having chemically reactive chloroacetamides as warheads, as well as an additional prodrug, **ML210**, that is converted to a nitrile oxide reactant in cells.[54] In a preliminary analysis of the cocrystalline structure of GPX4 with its covalent inhibitor **ML162** in a monomer model,[55] we noted that the solvent-exposed area of the ligand **ML162** exceeds 60%, especially in terms of rings A and C (Fig. 2B). Assuming that the under-occupied lipophilic pocket around rings A and C may be able to accommodate the ferrocenyl sandwich motif, this could provide an approach towards targeting GPX4 by ferrocene-appended GPX4 inhibitors.

To this end, 18 covalent GPX4 inhibitors with a ferrocenyl substituent incorporated at varied positions were synthesized so as to replace the aromatic ring of **ML162**, **RSL3** and **ML210**, as shown in Fig. 2B. Efficient syntheses of the designed ferrocenyl dipeptide analogues **10–17** proceeded in moderate to good yields, each *via* a Ugi four-component reaction from a diversity of reactants, aryl aldehydes, amines, carboxylic acids and isocyanides (Scheme S2†). The synthesis of ferrocenyl **RSL3** derivatives **18–21** was accomplished by Pictet–Spengler condensation of tryptophan analogues with formylferrocene, followed by an amide coupling (Scheme S3†). It took several steps to prepare the third series, and ferrocenyl compounds **22–27** were each obtained in a multi-step process (Scheme S4†). Benzoylferrocene derivatives were first prepared by a Friedel–Crafts acylation and then reduced, using sodium borohydride, to the corresponding alcohols **FC-2a/2b**. Treatment of **FC-2a/2b** with acetic anhydride provided the ester analogues, and was followed by treatment with excess piperazine in refluxing acetonitrile to afford **FC-3a/3b**. Coupling of secondary amines **FC-3a/3b** with carboxylic acids or acyl chlorides in dichloromethane delivered the final compounds **22–27**. The molecular structures of **12**, **15** and **17** were unequivocally established by X-ray crystallography, as illustrated in Fig. 2C and Tables S5–S8.†

In vitro anticancer evaluations and cellular uptake measurements

As mentioned above, a preliminary screening on ferroptosis-sensitive HT1080 cells, with or without fer-1, has been routinely used to evaluate the anticancer activity of our

Table 1 Antitumor activities and ferroptosis selectivity of target compounds towards HT1080 cells

Comp.		R_1	R_2	R_3	R_4	HT1080, IC_{50}[a] (μM) −fer-1	HT1080, IC_{50}[a] (μM) +fer-1	Selectivity[b]
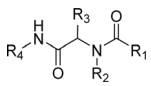	**10**					1.044 ± 0.201	1.699 ± 0.014	1.6
	11					4.980 ± 0.954	6.732 ± 1.228	1.4
	12				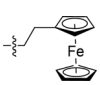	2.520 ± 0.290	1.749 ± 0.238	0.7
	13					4.866 ± 1.087	2.982 ± 0.667	0.6
	14					1.449 ± 0.069	4.068 ± 0.520	2.8
	15					0.043 ± 0.007	2.772 ± 0.231	64.5
	16			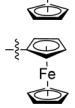		8.510 ± 1.371	9.391 ± 0.459	1.1
	17			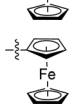		0.007 ± 0.001	1.486 ± 0.193	212.3
ML162						0.036 ± 0.013	2.200 ± 1.320	61.1

[a] Values are expressed as the mean of three independent experiments ± SD. [b] Selectivity: HT1080 IC_{50} with fer-1/HT1080 IC_{50} without fer-1.

molecules (as shown in Table 1). Encouragingly, in the case of **ML162** analogues, the designed compound **15** with a ferrocenyl group instead of 2-thienyl showed comparable antitumor activity and ferroptosis selectivity to that of **ML162**. However, introducing the ferrocenyl group at either the R_2 or R_4 position on the dipeptide scaffold of **ML162** seems to have a negative influence on both the antitumor activity and the ferroptosis selectivity. Compounds **10–14** displayed only moderate cytotoxicity on HT1080 cells without significant ferroptosis selectivity. More interestingly, the ferroptosis-inducing ability of dipeptide analogues bearing a ferrocenyl group can be modulated by changing the covalent warhead. Compound **17** possessing a propiolamide as its warhead showed a large improvement in antitumoral activity on HT1080 with IC_{50} values at the nanomolar level as well as excellent ferroptosis selectivity. However, replacing chloroacetamide with acrylamide, as in **16**, resulted in a very dramatic loss of activity relative to that of **ML162**. The best combination therefore appears to be a ferrocenyl group at the R_3 position and a propiolamide as the warhead.

In contrast to the diverse role of ferrocene in the antitumor behavior of **ML162**, incorporation of the ferrocenyl unit in **RSL3** and **ML210** by replacing the phenyl with ferrocenyl generally triggers a global loss of activity (as shown in Table S9†). In particular, in the analogues of **ML210**, all synthesized compounds bearing ferrocene show diminished ferroptosis-inducing activity, even with varied covalent warheads. One should note that, in the **RSL3** series, only ferrocenyl complex **21** possessing a propiolamide warhead exhibited approximately two-fold decreased antitumor activity, and five-fold reduced ferroptosis selectivity, compared to that of **RSL3**. These data emphasized the complexity of the effect of ferrocene on these three classical ferroptosis inducers in terms of their antitumoral activities and ferroptosis selectivity.

Inspired by the above results, we next attempted to evaluate the cytotoxicity effects of certain molecules on more cancers including ferroptosis-susceptible human renal cell carcinoma (OS-RC2), triple negative mouse breast cancer (TNBC 4T1), as well as two non-tumorigenic cell lines (L02 and MCF-10A), as shown in Table 2. OS-RC2 cells display high vulnerability to ferroptosis and are widely used to evaluate the specificity of compounds to ferroptosis, and the inhibitory activities of compounds against the GPX4 enzyme were evaluated on this cell line at 1 μM. Gratifyingly, ferrocene-appended compounds **15** and **17** exhibited outstanding ferroptosis selectivity and potent inhibition of GPX4 function, which was validated upon the exceptional reversal of cytotoxicity by the ferroptosis inhibitor. These data were in line with their antitumoral behaviors on the aforementioned ferroptosis-sensitive HT1080 cells. It is interesting to see that compounds **12** and **13**, each with a ferrocene group at the R_4 position on the **ML162** scaffold, bring about more vulnerability on OS-RC2 cells than HT1080 cells, and these two compounds also possess certain inhibitory activity on the GPX4 enzyme. This indicated that the growth of OS-RC2 may be more dependent on the function of GPX4. This phenomenon has also been observed for the ferrocene-appended RSL analogue **21** which has remarkable ferroptosis-inducing ability on OS-RC2 with a selectivity of 103.9 superior to that of HT1080. An obvious decrease in the cytotoxic activity was observed in the case of active derivatives on TNBC 4T1 cells, which indicated the distinctive damage wrought by ferroptosis on multiple cancer cells. On the other hand, compounds **15** and **17** display weaker cytotoxicity on human normal cells of L02 and MCF-10A compared to that of **ML162**, and this criterion indicates that they may be good candidates for drug development.

To comprehensively understand the synergistic effects between ferrocene and GPX4 inhibitors on these dual-function inducers, we then explored whether a simple combination of ferrocene compounds and GPX4 inhibitors could enhance ferroptosis induction and antitumor effects. As shown in Fig. S10,† the combination of ferrocene with **ML162** only resulted in identical inhibition compared with **ML162** alone on HT1080 cells; these antitumor effects are obviously weaker than those of the ferrocene-appended GPX4 inhibitor, **17**. These results acknowledged that the synergies of ferrocene and GPX4 inhibitors exert stronger ferroptosis inducing activities. In addition, ferrocenyl groups have been recognised as important

Table 2 Antitumor activities and ferroptosis selectivity of selected compounds on other cell lines: human renal cell carcinoma (OS-RC2), triple negative mouse breast cancer (4T1), normal liver cells (L-02) and normal breast cells (MCF-10A)

Comp.	OS-RC2, IC_{50}[a] (μM)		Selectivity[b]	GPX4 inhibition (%) at 1.0 μM	4T1 IC_{50} (μM)	L02 IC_{50} (μM)	MCF-10A IC_{50} (μM)
	−fer-1	+fer-1					
12	0.055 ± 0.017	10.16 ± 0.28	185	25.40 ± 4.24	0.634 ± 0.074	4.98 ± 0.87	NT
13	0.027 ± 0.003	2.42 ± 0.70	89.6	42.37 ± 1.93	0.192 ± 0.008	14.87 ± 5.78	7.81 ± 0.49
15	0.023 ± 0.005	7.687 ± 0.030	334.2	34.02 ± 4.94	0.169 ± 0.008	15.38 ± 4.35	7.79 ± 0.44
17	0.009 ± 0.001	6.917 ± 1.211	768.6	49.16 ± 4.60	0.095 ± 0.006	3.54 ± 0.56	7.32 ± 0.30
18	4.805 ± 0.364	4.281 ± 0.275	0.9	17.88 ± 1.03	NT	4.04 ± 0.79	NT
19	6.584 ± 0.442	4.023 ± 0.307	0.6	12.80 ± 2.67	NT	9.98 ± 2.69	NT
20	26.320 ± 0.930	25.560 ± 0.515	0.9	17.60 ± 11.13	12.930	15.76 ± 2.78	NT
21	0.028 ± 0.003	2.909 ± 0.589	103.9	15.74 ± 0.34	2.63 ± 0.6	4.27 ± 1.55	6.77 ± 0.11
ML162	0.021 ± 0.009	2.574 ± 0.49	122.3	45.02 ± 1.40	0.516 ± 0.059	1.20 ± 0.26	2.93 ± 0.12
RSL3	0.024 ± 0.004	0.69 ± 0.32	28.8	46.14 ± 5.44	0.34 ± 0.062	0.89 ± 0.13	16.93 ± 1.40

[a] Values are expressed as the mean of three independent experiments ± SD. [b] Selectivity: OS-RC2 IC_{50} with fer-1/OS-RC2 IC_{50} without fer-1.

hydrophobic organometallic units to improve the penetration of the cell membrane in terms of biologically active compounds;[56] the improvement of this effect is of interest to investigate for the compounds herein. The cellular uptake efficiency of **ML162** and **17** were examined by the LC-MS/MS method (Fig. S11†), which demonstrates that both complexes accumulate rapidly within cells on a time scale of hours. The internalization of **17** is significantly fast compared with that of **ML162** and leads to higher concentration inside of cells. As a consequence, the higher cytotoxicity of **17** may at least partly emerge from its high cellular accumulation due to the lipophilic ferrocenyl group.

Cell death and EMT process studies

To investigate the ferroptosis selectivity of ferrocene-appended GPX4 inhibitors, their modes of cell death were explored by employing the apoptosis inhibitor Z-VAD-FMK, the necrosis

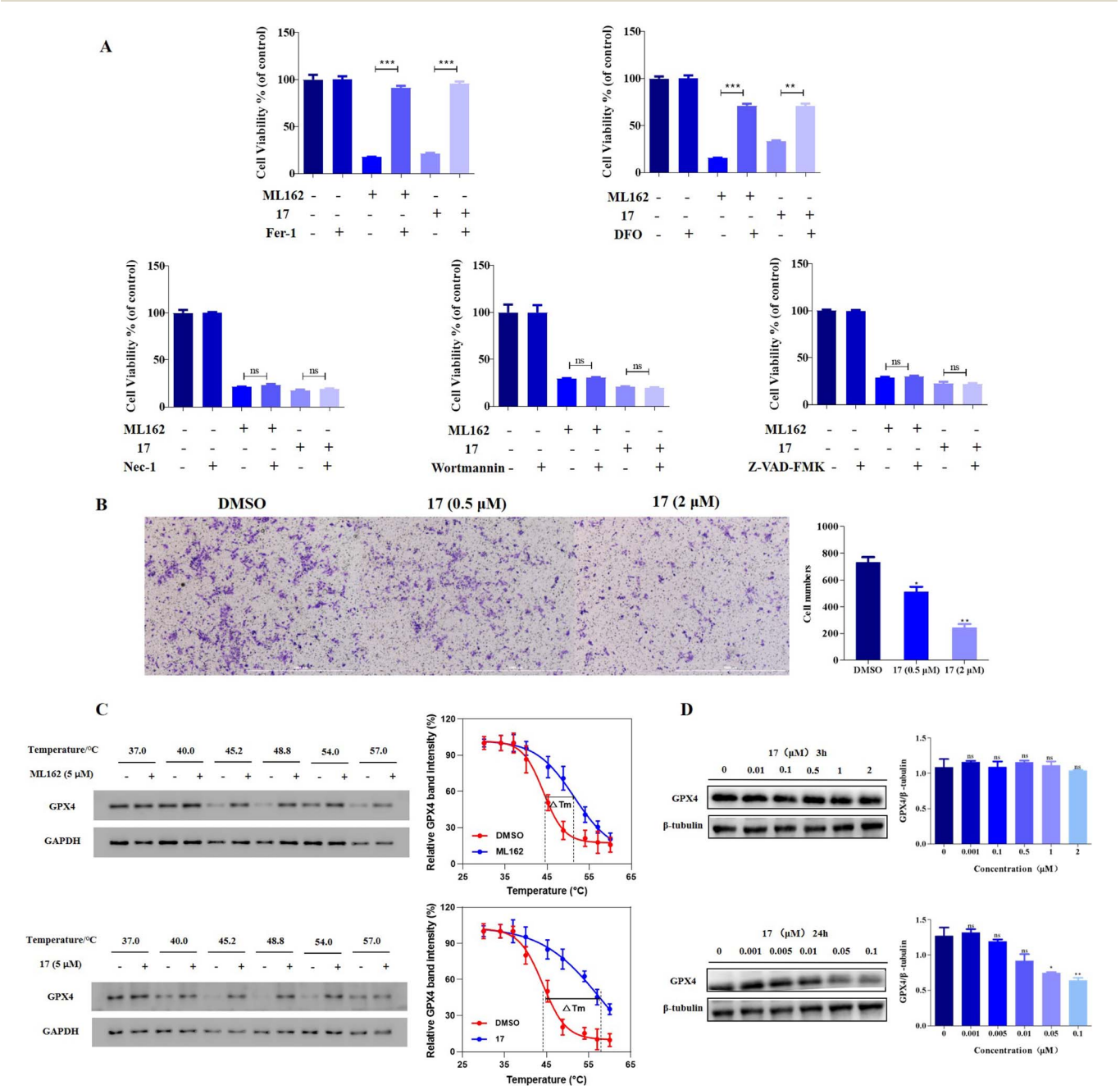

Fig. 3 (A) The percentage of cell viability after treatment of **ML162** or **17** (0.4 μM) with Z-VAD-FMK (10 μM), Nec-1 (10 μM), Wortmannin (30 μM), Fer-1 (2 μM), and DFO (30 μM); analysis results represented the mean ± SD. (B) Transwell assays were used to detect the invasion of cancer cells after treatment of **17** (0.5 and 2 μM). (C) CETSA experiments were performed on OS-RC-2 cells treated with DMSO, **ML162** and **17** (5 μM) for 4 h. The protein levels were analyzed by western blotting after heating at different temperatures (30–60 °C), and the apparent T_{agg} values for GPX4 in OS-RC-2 cells in the absence and presence of **ML162** and **17** were 44.09 °C to 51.42 °C, and 44.05 to 58.00 °C, respectively. (D) Western blot analysis of GPX4 levels in OS-RC-2 cells following treatment of **17** in 3 and 24 h. *$P < 0.05$, **$P < 0.01$, and ***$P < 0.001$ *versus* the control groups.

inhibitor necrostatin-1 (Nec-1), the autophagy inhibitor Wortmannin and the typical ferroptosis inhibitors fer-1 and deferoxamine (DFO). As shown in Fig. 3A, the percentage of cell viability of OS-RC2 upon combining the ferrocene-appended molecule **17** and the apoptosis inhibitor Z-VAD-FMK remained unchanged, indicating that **17** could not induce cell apoptosis at the current concentration. Moreover, the co-treatment of **17** with Nec-1 and Wortmannin, respectively, did not significantly thwart the cellular death of OS-RC2 induced by these two compounds. This demonstrated that the cellular death caused by **17** may not be attributable to necrosis and autophagy. In contrast, when combined with typical ferroptosis inhibitors fer-1 and DFO, the cytotoxicity of **17** was obviously reversed. Of particular note are the higher EC_{50} values of

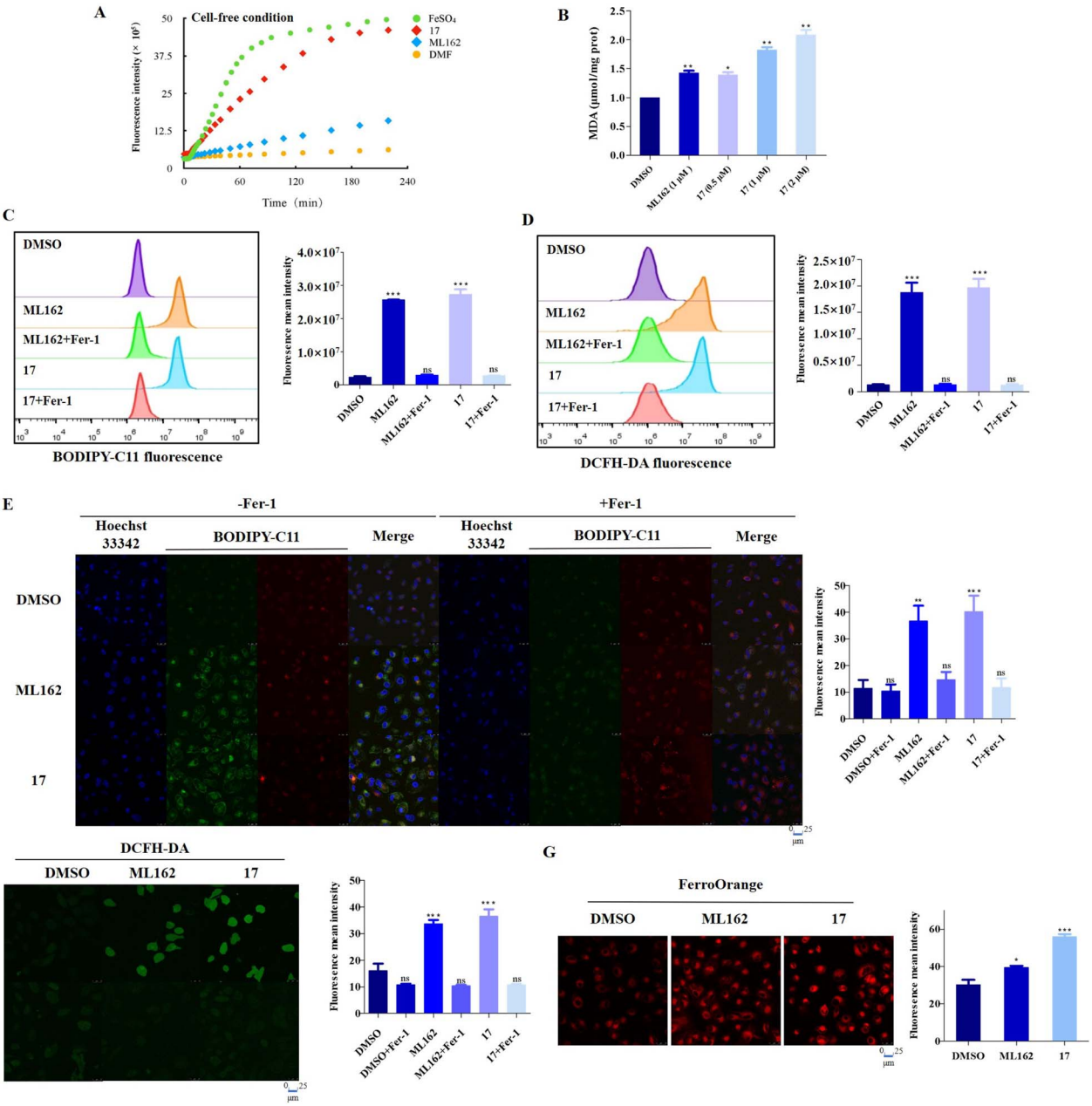

Fig. 4 (A) Monitoring of the generation of ROS of corresponding compounds (100 μM) using fluorescence spectroscopy in combination with ROS-sensitive DCFH-DA (λ_{ex} = 501 nm and λ_{em} = 531 nm). (B) OS-RC2 cells were treated with **ML162** (1 μM) and **17** (0.5, 1, and 2 μM) for 4 h, and then the content of MDA was determined. (C) Flow cytometry analysis for intracellular LPO by C11-BODIPY of OS-RC-2 cells treated with DMSO, **ML162** and **17** (0.5 μM) with and without fer-1 (1.5 μM) respectively. (D) Flow cytometry analysis for intracellular ROS by DCFH-DA of OS-RC-2 cells treated with DMSO, **ML162** and **17** (0.5 μM) with and without fer-1 (1.5 μM) respectively. (E) Representative confocal images and analysis of C11-BODIPY staining of OS-RC-2 cells after incubation with **ML162** and **17** (0.5 μM) with and without fer-1 (1.5 μM) respectively. (F) Representative confocal images and analysis of DCFH-DA staining of OS-RC-2 cells after incubation with **ML162** and **17** (0.5 μM) with and without fer-1 (1.5 μM) respectively. (G) Intracellular Fe^{2+} was visualized with the FerroOrange fluorescent probe. OS-RC-2 cells were treated with **ML162** and **17** (0.5 μM) for 4 h, and the content of intracellular Fe^{2+} was determined. *P < 0.05, **P < 0.01, and ***P < 0.001 *versus* the control groups.

ferroptosis inhibitors to reverse the cellular death posed by **17** compared to that of **ML162** (Table S10†); these observations confirmed that the potent antiproliferative activities of **17** were achieved mainly by inducing ferroptosis of cancer cells, and also underscored its remarkable ferroptosis selectivity.

EMT is connected to carcinogenesis, invasiveness, metastasis, and therapeutic resistance in cancer. Increasing evidence shows that cancer cells undergoing EMT are vulnerable to ferroptotic cell death.[11,12] Thus, the effect of the ferroptosis-inducing agent **17** on the migration and invasion of cancer cells was examined. Through a wound-healing assay, it was found that those compounds significantly prevented the migration of 4T1 cells time-dependently, especially in the case of **17** (Fig. S11†). Similarly, transwell assays revealed that this molecule disrupts the invasion of tumor cells dose-dependently (Fig. 3B). These results indicated the superior capacity of ferrocene-appended ferroptosis inducers to block the migratory and invasive properties of 4T1 cells, denoting their enormous promise for the treatment of refractory cancer metastasis, taking into account that TNBC 4T1 cells have high invasiveness, and approximately half of the TNBC cases will have distant metastasis.[57]

GPX4 CETSA and western blotting evaluations

Since certain ferrocene-appended molecules exhibited high selectivity for ferroptosis and remarkable GPX4 inhibition activities, the effect of **17** on an intact GPX protein was further determined, and the results are shown in Fig. 3C and D. The ability of **17** for binding GPX4 was first validated by the cellular thermal shift assay (CETSA) considering that the stability of the protein is changed when it is bound with the molecule. It was found that the aggregation temperature (T_{agg}) of GPX4 was improved by ~14 °C in OS-RC2 cells after treatment of **17**, whereas the T_{agg} in the case of **ML162** increased by ~7 °C, indicating the stronger interaction of **17** with GPX4 in the cells. The increased thermal stability of GPX4 is in line with that of **ML210** and other alkyne analogues on the stabilization of GPX4 reported previously,[54] suggesting that they may bind to GPX4 in a similar way. Meanwhile, the expression level of GPX4 was further investigated by western blot, and it is noteworthy that there was no obvious difference in the protein level of GPX4 compared to that of the control group within 3 h of **17** treatment (Fig. 3D). However, the down-regulation of GPX4 was evident after 24 h treatment. One could speculate that the potent ferroptosis-inducing ability of ferrocene-based **ML162** analogues may result from both the inhibition and down-grading of GPX4 during long-term cellular incubation. These results accentuate the complex effects of covalent inhibitors on GPX4.

LPO related bioactivity evaluations

It is well known that certain ferrocene complexes can induce the formation of ROS *via* a Fenton type reaction. Therefore, the ability of ferrocene-appended GPX4 inhibitor **17** to yield ROS was first evaluated under physiological conditions by the widely used fluorescent ROS indicator, 2′,7′-dichlorofluorescein diacetate (DCFH-DA). As shown in Fig. 4A, a known H_2O_2-induced activation method was carried out to monitor the ROS generation by using selected molecules in buffer,[47] containing $FeSO_4$ as a positive control. It is evident that **17** can facilitate the conversion of H_2O_2 to $OH^{\bullet}$ and increase the production of ROS in a time-dependent manner, reflected by the $OH^{\bullet}$-mediated oxidation of nonfluorescent 2′,7′-dichlorofluorescein (DCFH) to fluorescent 2′,7′-dichlorofluorescein (DCF). In contrast, the pure organic compound **ML162** did not exhibit obvious catalytic efficiency for yielding ROS. Unrestricted lipid peroxidation is a hallmark of ferroptosis, which can be evaluated in cells by multiple approaches. As a metabolite of LPOs, the level of MDA is commonly used as a characteristic index for the determination of LPOs. As illustrated in Fig. 4B, **17** improved the contents of MDA in cells dose-dependently and more prominently than **ML162** at the same concentration, which corresponds to the phenomenon observed at the molecular level.

Accordingly, the fluorescent probes C11-BODIPY and DCFH-DA were employed to investigate the intracellular ROS and LPOs *via* flow cytometry and confocal laser scanning microscopy (CLSM). As illustrated in Fig. 4C and D, **17** could significantly induce the accumulation of LPOs slightly more than **ML162** and this trend could be reversed by fer-1 totally according to the flow cytometry analysis, which emphasized its remarkable ferroptosis selectivity. In agreement with this, the oxidative fluorescence intensity (green) of C11-BODIPY and DCFH-DA in OS-RC2 cells significantly increased upon treatment with **17** (Fig. 4E and F). Considering the iron dependence which can make cancer cells more vulnerable to ferroptosis, the overall level of cellular ferrous iron was detected by Fe^{2+}-sensitive FerroOrange staining. As shown in Fig. 4G, the images of FerroOrange staining

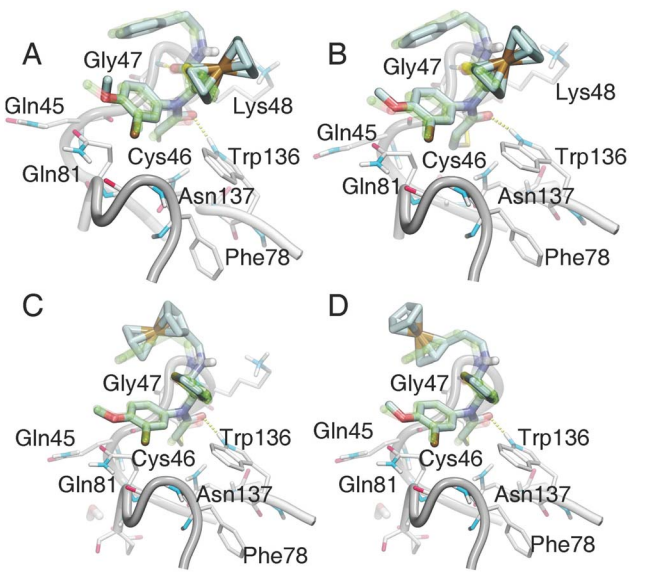

Fig. 5 The binding models of ferrocenyl ligands in the GPX4 crystal structure (PDB code 6HKQ). Compounds **15** (A), **17** (B), **12** (C), and **13** (D) were docked to GPX4 by Watvina with the template-based method; then all the structures were minimized with the xtb program. The original ligand ML162 was shown in green transparent stick mode, and ferrocenyl ligands in cyan stick mode. The hydrogen bonds were represented with a yellow dashed line by VMD software.

intuitively illustrated that a notable fluorescence intensity of the cells after treatment with **17** is found to be significantly higher than that of cells incubated with **ML162**, suggesting that **17** can increase the level of cellular ferrous iron. Overall, these results verified by the increasing LPOs and Fe^{2+}, lead to a consistent conclusion that ferrocene-appended GPX4 inhibitors could significantly induce the accumulation of LPOs and subsequently engender severe ferroptosis of cancer cells.

Molecular docking

The molecular simulation of small molecular ligands with GPX4 has been challenging due to the flat surface surrounding the active site of GPX4,[58] and thus a template-based docking by Watvina was carried out. According to the atomic types and their contribution to ligand–receptor interaction, we first generate a template-containing mapping of heavy atoms, aromatic atoms and hydrogen bond receptors (Fig. S12†). Using the genetic algorithm for global searching and BFGS for local refinement in Watvina, the conformation with the highest template matching score of docked ferrocene derivatives was used for further analysis. As shown in Fig. 5, the selected ligands **12**, **13**, **15** and **17** docked well to the **ML162** space with a paired atom RMSD of less than 0.5 Å. These four organometallics enabled the formation of two key hydrogen bonds with residues of GPX4 like that of **ML162**. One of the cyclopentadienyl rings of **15** or **17** occupied the same hydrophobic space as that of **ML162**, and the resulting conformation of **17** revealed that it filled the active pocket better than compound **15**. In the case of **12** and **13**, the ferrocene groups are placed *in lieu* of the benzene (ring C) part in **ML162** (Fig. 2B, 5C and D). Since ring C occupied by ferrocene is flexible and distal from the binding pocket, **12** and **13** may exhibit weak binding activity with GPX4. As for compounds **10** and **11** with the ferrocenyl group sited at the very cramped ring B part (Fig. 2B), they were expected to lose the capacity of conjugating GPX4. Indeed, these docking data, which held the binding mode of covalent inhibitors with GPX4, concur well with their GPX4 inhibitory activities and thus provided a reasonable interpretation.

In vivo profiling of ferrocene-based ferroptosis inducers

Considering the excellent antitumor activities of **17** on two ferroptosis sensitive cell lines, the OS-RC2 xenograft model was

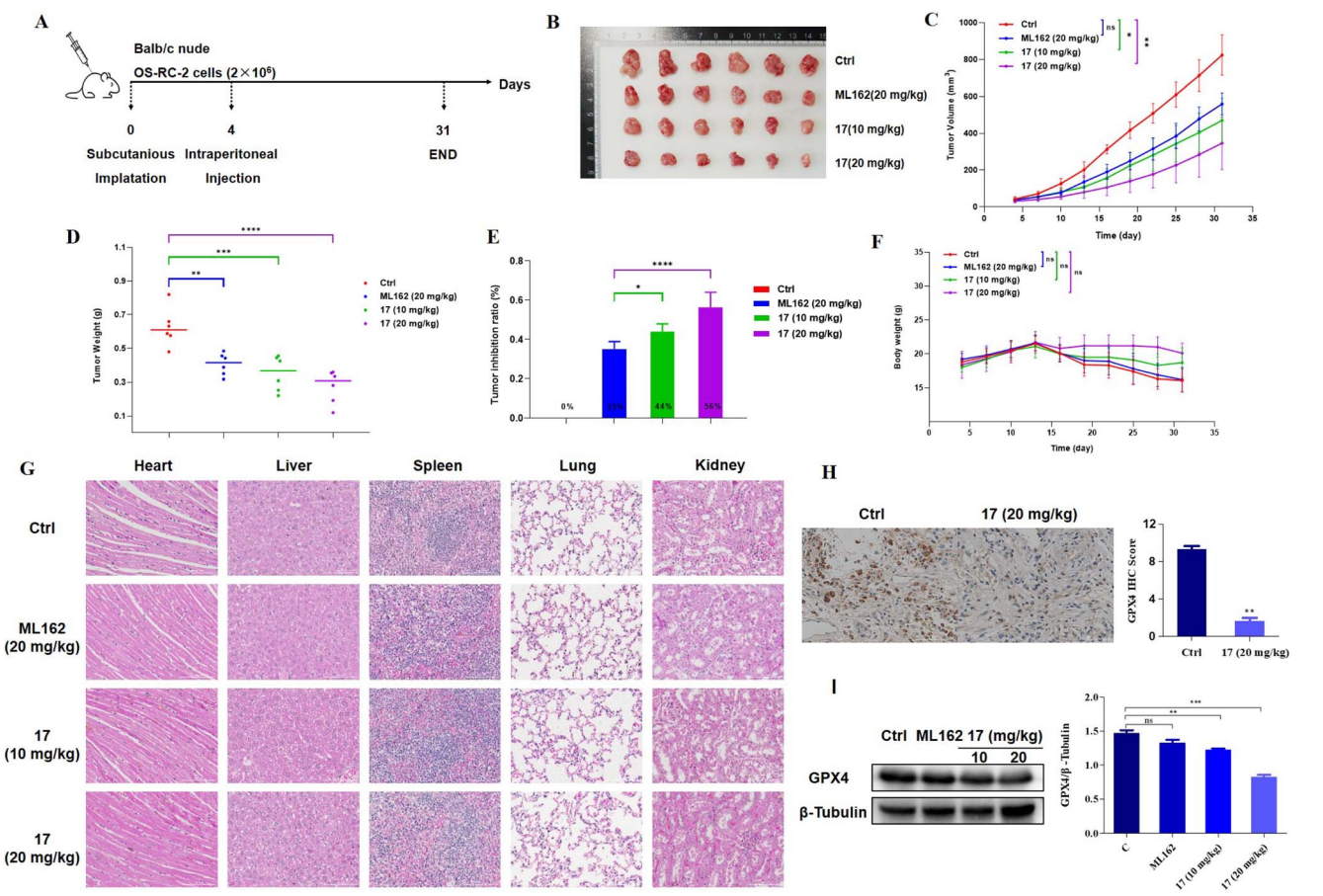

Fig. 6 (A) *In vivo* antitumor activity of **ML162** and **17** in a human OS-RC2 renal carcinoma model (BALB/c nude mice, given medicine every three days, $n = 6$). (B) Picture of excised tumors from the different groups after the treatment; (C) tumor volume curves during the treatment period; (D) tumor weights after treatment; (E) tumor inhibition ratio after the treatment period. (F) Body weight curves of different groups after the treatment; (G) H&E staining of the major organs of mice after treatment with compounds. (H) Anti-GPX4 immunohistochemistry images and analysis from the OS-RC-2 xenograft model. (I) Western blot analysis of GPX4 levels in tumor tissue following treatment of the corresponding compounds. *$P < 0.05$, **$P < 0.01$, ***$P < 0.001$ and ****$P < 0.0001$ *versus* the control groups.

established in BALB/C nude mice to assess its *in vivo* efficacy. The tested compounds were administered by intraperitoneal injection every three days for approximately 4 weeks (Fig. 6). The tumor growth inhibition (TGI) values of **17**-treated groups were 44%@10 mg kg^{-1} and 56%@20 mg kg^{-1}, which showed that **17** could suppress the progression of the renal tumor with a significant dose-dependent effect. It is noteworthy that **17** displayed prominent antitumor activities *in vivo* compared to **ML162** in the same case of delivering a high dose of drugs. Additionally, there was no obvious difference in body weight of the **17** treatment groups compared with the control group. Furthermore, hematoxylin and eosin (H&E) staining analysis of the major organs was carried out to investigate the safety profile of **ML162** and **17**, which indicated that there was no apparent toxic damage observed in major organs such as the heart, liver, spleen, lung, and kidney. Subsequent immunohistochemical analysis and western blot studies showed that **17** evidently reduced the level of the GPX4 protein in tumor tissues, revealing that ferrocenyl complex **17** effectively induced ferroptosis *in vivo*. These results emphasized the superior potential of ferrocene-based ferroptosis inducers as anticancer drug candidates for further research.

RNA-seq analysis

To further illustrate the impact of **17** on the gene expression pattern, we employed the NovaSeq 6000 PE150 platform

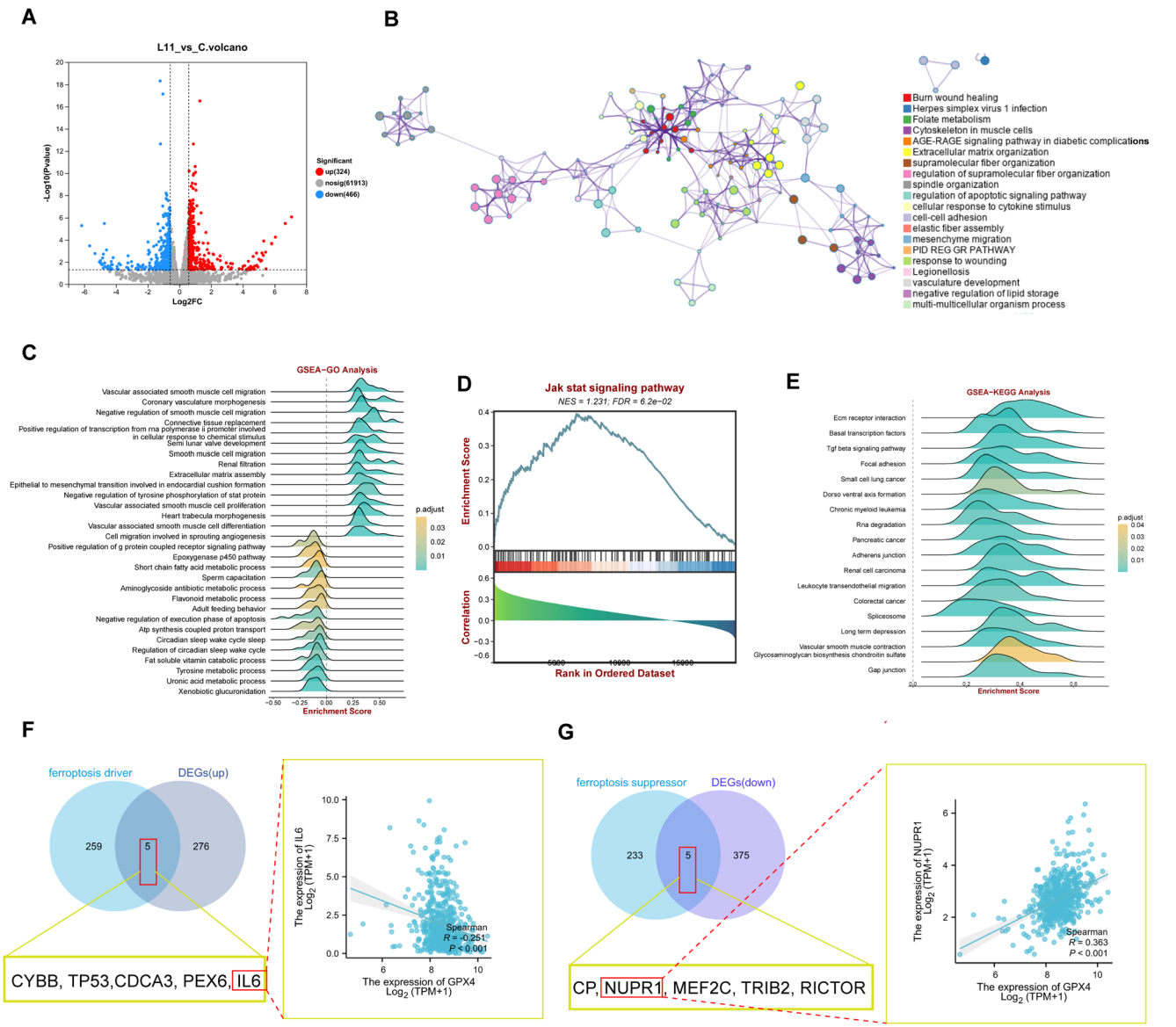

Fig. 7 RNA-seq analysis of samples from OS-RC-2 xenograft model rats treated with **17** (20 mg kg^{-1}) and the control. (A) Volcano plot of all DEGs; red indicates upregulation, whereas blue indicates downregulation. (B) Protein–protein interaction (PPI) networks constructed by Metascape and the protein function were enriched. (C) GO term enrichment analysis of DEGs from the **17** (20 mg kg^{-1}) treatment group. (D) GSEA analysis of DEGs in the JAK-STAT signaling pathway. (E) KEGG enrichment analysis of DEGs from the **17** (20 mg kg^{-1}) treatment group. (F and G) The genes as the driver and suppressor of ferroptosis overlap with DEGs that are up-regulated and down-regulated by using a Venn diagram.

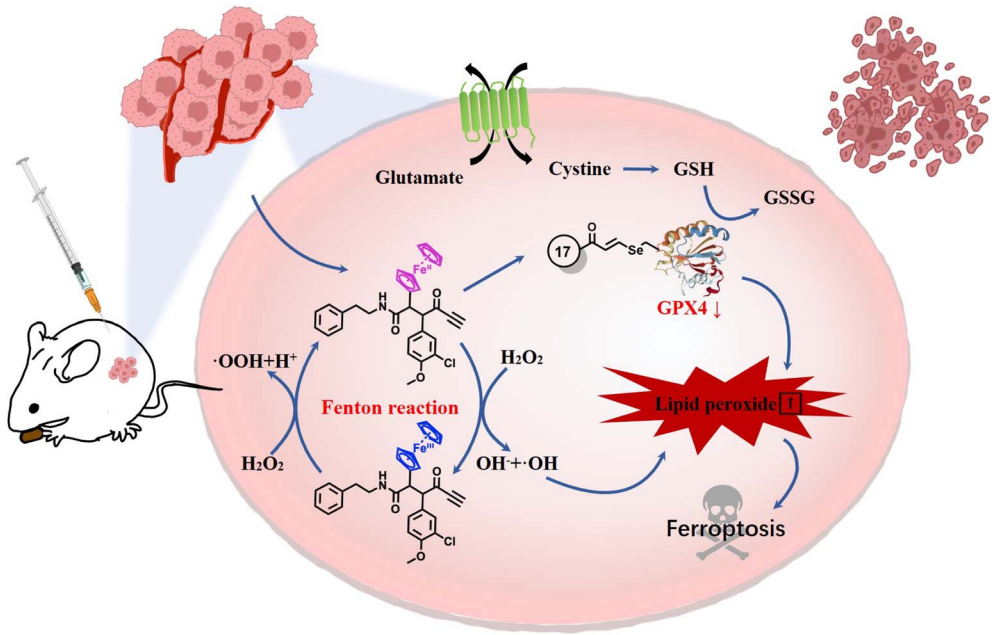

Fig. 8 Proposed mechanisms of ferrocene-appended ferroptosis inducers.

(Illumina Inc., CA, USA) to analyze gene expression differences (DEGs) between the extracts of tumor tissues from OS-RC-2 xenograft model rats treated with **17** (20 mg kg^{-1}) and normal control rats. A volcano plot illustrated significant differences in mRNA expression patterns between the two groups (Fig. 7A and Table S13†). Utilizing the Limma package, we identified differential genes under the condition p-value < 0.05 & |log FC| > 1, resulting in 790 differentially expressed genes (324 up-regulated and 466 down-regulated).

Subsequently, we constructed a PPI network of the 790 DEGs using Metascape. This analysis revealed enrichment in ferroptosis-related signaling pathways and cell phenotypes, including folate metabolism, the AGE-RAGE signaling pathway in diabetic composites, negative regulation of lipid storage, and mesenchymal migration (Fig. 7B). Further insight into the biological functions and signaling pathways associated with ferroptosis was gained through GO and KEGG analyses (Fig. 7C–E). These analyses demonstrated the involvement of DEGs in multiple biological processes related to iron homeostasis, such as cyclooxygenase and G protein-coupled receptor signaling pathways. Notably, the activation of multiple inflammation-related signaling pathways leading to ferroptosis was observed, with DEGs enriched in the inflammatory signaling pathway Jak-stat, as indicated by GSVA analysis (Fig. 7D). KEGG analysis also highlighted involvement in pathways related to iron and lipid metabolism, including short-chain fatty acid metabolism and tyrosine metabolism (Fig. 7E). To explore the correlation of **17** with ferroptosis-related pathways, we examined the overlapping genes between the ferroptosis driver and DEGs, or ferroptosis suppressor genes and DEGs after **17** treatment. The results revealed that **17** upregulated ferroptosis driver genes (CYBB, TP53, CDCA3, PEX6, and IL6) and down-regulated suppressor genes (CP, NUPR1, MEF2C, TRIB2, RICTOR, including GPX4). The correlation analysis showed a significant negative correlation between the driving gene IL6 and GPX4 (Fig. 7F) and a significant positive correlation with UPR1 and GPX4 (Fig. 7G), indicating the targeted inhibition of GPX4 function by **17** to induce ferroptosis in renal cell carcinoma *in vivo*.

Conclusions

According to the ferroptosis-based phenotypic screening of our in-house organometallic compound library, the usual ferrocene complexes did not possess visible ferroptosis-inducing activities, which contradicted the conventional understanding of ferrocene for ferroptosis. As a result, a series of ferrocene-appended GPX4 inhibitors has been rationally designed by a one-stone-two-birds strategy for the first time. Distinct from the known bioferrocene species, only using the ferrocenyl group as an auxiliary fragment for existing organic moieties, or merely taking advantage of the redox behaviors of ferrous iron to generate ROS, complex **17** can both inhibit GPX4 effectively and catalyze the Fenton-like reaction to yield ROS, and consequently result in stronger antiproliferative activity and higher ferroptosis selectivity than the corresponding organic compound **ML162** (Fig. 8). Therefore, as a proof-of-concept study, we successfully achieved the goal to use a single molecule to modulate the two main pathways of ferroptosis, iron homeostasis and the antioxidant defense system. In particular, cellular CETSA experiments confirmed the strong interaction of **17** with an intact GPX4 protein, and this result was in accordance with its capability to disrupt the function of GPX4 in OS-RC2 cells. Moreover, the significant ROS-inducing ability of **17** at both the molecular level and at the cellular level acknowledged the ferroptosis enhancement of the ferrocene-appended GPX4

inhibitor. Subsequent *in vivo* experiments demonstrated that **17** is a potent attenuator of the growth of renal tumors, and ferroptosis is pronounced to be involved in this inhibition process, supported by the GPX4 content analysis and RNA-seq study of tumor tissues. In conclusion, we present here a comprehensive study of rationally designed ferrocene-appended ferroptosis inducers, not only to promote the development of ferroptosis-based anticancer treatments, but also to provide new insight into the design of novel bioorganometallics based on ferrocene for potential disease therapies.

Data availability

The data that support the findings of this study are available in the ESI† or on request from the corresponding author.

Author contributions

W. L., J. Y., J. W. and X. F. contributed equally to this manuscript. Y. W. and J. L. designed the study. W. L., J. W., H. W. and Q. Z. performed the synthesis and characterization of the chemical compounds. J. Y., X. F., Y. X., X. Z. and X. Qi performed the *in vitro* and *in vivo* anticancer evaluation of the compounds. X. X. performed the docking calculation work. X. L. and X. Qiu contributed to the target protein binding affinity evaluation. P. P., Q. G., G. J. and S. Y. contributed to the construction of the ferrocene-based compound library. J. B.-C. and M. J. M. prepared the crystal figure. Y. W., J. L. and X. Qiu supervised the study. Y. W., J. L. and M. J. M. wrote the manuscript. All authors participated in valuable discussion and manuscript correction.

Conflicts of interest

Y. W., J. L., J. W., W. L., H. W. and X. Z. are inventors on a patent application related to this work.

Acknowledgements

Y. W. received funding from Qingdao Marine Science and Technology (2022QNLM030003-2), Taishan Scholar Youth Expert Program in Shandong Province (tsqn202103035) and the Distinguished Young Scholars of Shandong Provincial Natural Science Foundation (Overseas, 2022HWYQ-069), andX. Q. is thankful for the support of the Fundamental Research Funds for the Central Universities of Ocean University of China (No. 202262015).

References

1 S. J. Dixon, K. M. Lemberg, M. R. Lamprecht, R. Skouta, E. M. Zaitsev, C. E. Gleason, D. N. Patel, A. J. Bauer, A. M. Cantley, W. S. Yang, B. Morrison III and B. R. Stockwell, Ferroptosis: An Iron-Dependent Form of Nonapoptotic Cell Death, *Cell*, 2012, **149**(5), 1060–1072.

2 K. Hadian and B. R. Stockwell, SnapShot: Ferroptosis, *Cell*, 2020, **181**(5), 1188.

3 B. R. Stockwell, Ferroptosis turns 10: Emerging mechanisms, physiological functions, and therapeutic applications, *Cell*, 2022, **185**(14), 2401–2421.

4 X. Fang, H. Wang, D. Han, E. Xie, X. Yang, J. Wei, S. Gu, F. Gao, N. Zhu, X. Yin, Q. Cheng, P. Zhang, W. Dai, J. Chen, F. Yang, H.-T. Yang, A. Linkermann, W. Gu, J. Min and F. Wang, Ferroptosis as a target for protection against cardiomyopathy, *Proc. Natl. Acad. Sci. U. S. A.*, 2019, **116**(7), 2672–2680.

5 W.-Y. Sun, V. A. Tyurin, K. Mikulska-Ruminska, I. H. Shrivastava, T. S. Anthonymuthu, Y.-J. Zhai, M.-H. Pan, H.-B. Gong, D.-H. Lu, J. Sun, W.-J. Duan, S. Korolev, A. Y. Abramov, P. R. Angelova, I. Miller, O. Beharier, G.-W. Mao, H. H. Dar, A. A. Kapralov, A. A. Amoscato, T. G. Hastings, T. J. Greenamyre, C. T. Chu, Y. Sadovsky, I. Bahar, H. Bayır, Y. Y. Tyurina, R.-R. He and V. E. Kagan, Phospholipase iPLA2β averts ferroptosis by eliminating a redox lipid death signal, *Nat. Chem. Biol.*, 2021, **17**(4), 465–476.

6 R. Skouta, S. J. Dixon, J. Wang, D. E. Dunn, M. Orman, K. Shimada, P. A. Rosenberg, D. C. Lo, J. M. Weinberg, A. Linkermann and B. R. Stockwell, Ferrostatins Inhibit Oxidative Lipid Damage and Cell Death in Diverse Disease Models, *J. Am. Chem. Soc.*, 2014, **136**(12), 4551–4556.

7 J. P. Friedmann Angeli, M. Schneider, B. Proneth, Y. Y. Tyurina, V. A. Tyurin, V. J. Hammond, N. Herbach, M. Aichler, A. Walch, E. Eggenhofer, D. Basavarajappa, O. Rådmark, S. Kobayashi, T. Seibt, H. Beck, F. Neff, I. Esposito, R. Wanke, H. Förster, O. Yefremova, M. Heinrichmeyer, G. W. Bornkamm, E. K. Geissler, S. B. Thomas, B. R. Stockwell, V. B. O'Donnell, V. E. Kagan, J. A. Schick and M. Conrad, Inactivation of the ferroptosis regulator Gpx4 triggers acute renal failure in mice, *Nat. Cell Biol.*, 2014, **16**(12), 1180–1191.

8 J. Li, J. Liu, Z. Zhou, R. Wu, X. Chen, C. Yu, B. Stockwell, G. Kroemer, R. Kang and D. Tang, Tumor-specific GPX4 degradation enhances ferroptosis-initiated antitumor immune response in mouse models of pancreatic cancer, *Sci. Transl. Med.*, 2023, **15**(720), eadg3049.

9 X. Jiang, B. R. Stockwell and M. Conrad, Ferroptosis: mechanisms, biology and role in disease, *Nat. Rev. Mol. Cell Biol.*, 2021, **22**(4), 266–282.

10 C. Mao, X. Liu, Y. Zhang, G. Lei, Y. Yan, H. Lee, P. Koppula, S. Wu, L. Zhuang, B. Fang, M. V. Poyurovsky, K. Olszewski and B. Gan, DHODH-mediated ferroptosis defence is a targetable vulnerability in cancer, *Nature*, 2021, **593**(7860), 586–590.

11 M. J. Hangauer, V. S. Viswanathan, M. J. Ryan, D. Bole, J. K. Eaton, A. Matov, J. Galeas, H. D. Dhruv, M. E. Berens, S. L. Schreiber, F. McCormick and M. T. McManus, Drug-tolerant persister cancer cells are vulnerable to GPX4 inhibition, *Nature*, 2017, **551**(7679), 247–250.

12 V. S. Viswanathan, M. J. Ryan, H. D. Dhruv, S. Gill, O. M. Eichhoff, B. Seashore-Ludlow, S. D. Kaffenberger, J. K. Eaton, K. Shimada, A. J. Aguirre, S. R. Viswanathan, S. Chattopadhyay, P. Tamayo, W. S. Yang, M. G. Rees, S. Chen, Z. V. Boskovic, S. Javaid, C. Huang, X. Wu,

Y. Y. Tseng, E. M. Roider, D. Gao, J. M. Cleary, B. M. Wolpin, J. P. Mesirov, D. A. Haber, J. A. Engelman, J. S. Boehm, J. D. Kotz, C. S. Hon, Y. Chen, W. C. Hahn, M. P. Levesque, J. G. Doench, M. E. Berens, A. F. Shamji, P. A. Clemons, B. R. Stockwell and S. L. Schreiber, Dependency of a therapy-resistant state of cancer cells on a lipid peroxidase pathway, *Nature*, 2017, **547**(7664), 453–457.

13 I. Ingold, C. Berndt, S. Schmitt, S. Doll, G. Poschmann, A. Roveri, X. Peng, F. P. Freitas, M. Aichler, M. Jastroch, F. Ursini, E. S. J. Arnér, N. Fradejas-Villar, U. Schweizer, H. Zischka, J. P. F. Angeli and M. Conrad, Selenium utilization by GPX4 was an evolutionary requirement to prevent hydroperoxide-induced ferroptosis, *Free Radical Biol. Med.*, 2017, **112**, 24.

14 B. Hassannia, P. Vandenabeele and T. Vanden Berghe, Targeting Ferroptosis to Iron Out Cancer, *Cancer Cell*, 2019, **35**(6), 830–849.

15 X. Chen, C. Yu, R. Kang and D. Tang, Iron Metabolism in Ferroptosis, *Front. Cell Dev. Biol.*, 2020, **8**, 590226.

16 M. Patra and G. Gasser, The medicinal chemistry of ferrocene and its derivatives, *Nat. Rev. Chem.*, 2017, **1**(9), 0066.

17 G. Jaouen, A. Vessieres and S. Top, Ferrocifen type anti cancer drugs, *Chem. Soc. Rev.*, 2015, **44**(24), 8802–8817.

18 B. Sharma and V. Kumar, Has Ferrocene Really Delivered Its Role in Accentuating the Bioactivity of Organic Scaffolds?, *J. Med. Chem.*, 2021, **64**(23), 16865–16921.

19 R. Wang, H. Chen, W. Yan, M. Zheng, T. Zhang and Y. Zhang, Ferrocene-containing hybrids as potential anticancer agents: Current developments, mechanisms of action and structure-activity relationships, *Eur. J. Med. Chem.*, 2020, **190**, 112109.

20 A. Vessières, Y. Wang, M. J. McGlinchey and G. Jaouen, Multifaceted chemical behaviour of metallocene (M = Fe, Os) quinone methides. Their contribution to biology, *Coord. Chem. Rev.*, 2021, **430**, 213658.

21 W.-J. Wang, Y.-Y. Ling, Y.-M. Zhong, Z.-Y. Li, C.-P. Tan and Z.-W. Mao, Ferroptosis-Enhanced Cancer Immunity by a Ferrocene-Appended Iridium(III) Diphosphine Complex, *Angew. Chem., Int. Ed.*, 2022, **61**(16), e202115247.

22 J. Li, Q. Zong, Y. Liu, X. Xiao, J. Zhou, Z. Zhao and Y. Yuan, Self-catalyzed tumor ferroptosis based on ferrocene conjugated reactive oxygen species generation and a responsive polymer, *Chem. Commun.*, 2022, **58**(20), 3294–3297.

23 X. Zhang, Y. Ding, Z. Zhang, Y. Ma, X. Sun, L. Wang, Z. Yang and Z.-W. Hu, In Situ Construction of Ferrocene-Containing Membrane-Bound Nanofibers for the Redox Control of Cancer Cell Death and Cancer Therapy, *Nano Lett.*, 2023, **23**(16), 7665–7674.

24 J. Sagasser, B. N. Ma, D. Baecker, S. Salcher, M. Hermann, J. Lamprecht, S. Angerer, P. Obexer, B. Kircher and R. Gust, A New Approach in Cancer Treatment: Discovery of Chlorido[N,N′-disalicylidene-1,2-phenylenediamine] iron(III) Complexes as Ferroptosis Inducers, *J. Med. Chem.*, 2019, **62**(17), 8053–8061.

25 M. Lv, Y. Zheng, J. Wu, Z. Shen, B. Guo, G. Hu, Y. Huang, J. Zhao, Y. Qian, Z. Su, C. Wu, X. Xue, H. K. Liu and Z. W. Mao, Evoking Ferroptosis by Synergistic Enhancement of a Cyclopentadienyl Iridium-Betulin Immune Agonist, *Angew. Chem., Int. Ed.*, 2023, **62**(48), e202312897.

26 B. Rosenberg and L. Vancamp, Successful Regression of Large Solid Sarcoma 180-Tumors by Platinum Compounds, *Cancer Res.*, 1970, **30**(6), 1799–1802.

27 J. J. Wilson and S. J. Lippard, Synthetic Methods for the Preparation of Platinum Anticancer Complexes, *Chem. Rev.*, 2014, **114**(8), 4470–4495.

28 T. Yang, S. Zhang, H. Yuan, Y. Wang, L. Cai, H. Chen, X. Wang, D. Song, X. Wang, Z. Guo and X. Wang, Platinum-Based TREM2 Inhibitor Suppresses Tumors by Remodeling the Immunosuppressive Microenvironment, *Angew. Chem., Int. Ed.*, 2023, **62**(2), e202213337.

29 X. Wang, X. Wang, S. Jin, N. Muhammad and Z. Guo, Stimuli-Responsive Therapeutic Metallodrugs, *Chem. Rev.*, 2019, **119**(2), 1138–1192.

30 X. Zhao, J. Zhang, W. Zhang, Z. Guo, W. Wei, X. Wang and J. Zhao, A chiral fluorescent Ir(iii) complex that targets the GPX4 and ErbB pathways to induce cellular ferroptosis, *Chem. Sci.*, 2023, **14**(5), 1114–1122.

31 R. Lengacher, Y. Wang, H. Braband, O. Blacque, G. Gasser and R. Alberto, Organometallic small molecule kinase inhibitors – direct incorporation of Re and 99mTc into Opaganib®, *Chem. Commun.*, 2021, **57**(98), 13349–13352.

32 S. M. Meier-Menches, C. Gerner, W. Berger, C. G. Hartinger and B. K. Keppler, Structure–activity relationships for ruthenium and osmium anticancer agents – towards clinical development, *Chem. Soc. Rev.*, 2018, **47**(3), 909–928.

33 X. Wang, M. d. G. Jaraquemada-Peláez, C. Rodríguez-Rodríguez, Y. Cao, C. Buchwalder, N. Choudhary, U. Jermilova, C. F. Ramogida, K. Saatchi, U. O. Häfeli, B. O. Patrick and C. Orvig, H4octox: Versatile Bimodal Octadentate Acyclic Chelating Ligand for Medicinal Inorganic Chemistry, *J. Am. Chem. Soc.*, 2018, **140**(45), 15487–15500.

34 H. Huang, S. Banerjee, K. Qiu, P. Zhang, O. Blacque, T. Malcomson, M. J. Paterson, G. J. Clarkson, M. Staniforth, V. G. Stavros, G. Gasser, H. Chao and P. J. Sadler, Targeted photoredox catalysis in cancer cells, *Nat. Chem.*, 2019, **11**(11), 1041–1048.

35 J.-J. Zhang, M. A. Abu el Maaty, H. Hoffmeister, C. Schmidt, J. K. Muenzner, R. Schobert, S. Wölfl and I. Ott, A Multitarget Gold(I) Complex Induces Cytotoxicity Related to Aneuploidy in HCT-116 Colorectal Carcinoma Cells, *Angew. Chem., Int. Ed.*, 2020, **59**(38), 16795–16800.

36 W. D. J. Tremlett, D. M. Goodman, T. R. Steel, S. Kumar, A. Wieczorek-Błauż, F. P. Walsh, M. P. Sullivan, M. Hanif and C. G. Hartinger, Design concepts of half-sandwich organoruthenium anticancer agents based on bidentate bioactive ligands, *Coord. Chem. Rev.*, 2021, **445**, 213950.

37 G. Moreno-Alcántar and A. Casini, Bioinorganic supramolecular coordination complexes and their biomedical applications, *FEBS Lett.*, 2023, **597**(1), 191–202.

38 D. R. van Staveren and N. Metzler-Nolte, Bioorganometallic Chemistry of Ferrocene, *Chem. Rev.*, 2004, **104**(12), 5931–5986.

39 K. Kowalski, Organometallic nucleosides—Synthesis, transformations, and applications, *Coord. Chem. Rev.*, 2021, **432**, 213705.

40 H.-G. Xu, M. Schikora, M. Sisa, S. Daum, I. Klemt, C. Janko, C. Alexiou, G. Bila, R. Bilyy, W. Gong, M. Schmitt, L. Sellner and A. Mokhir, An Endoplasmic Reticulum Specific Pro-amplifier of Reactive Oxygen Species in Cancer Cells, *Angew. Chem., Int. Ed.*, 2021, **60**(20), 11158–11162.

41 J. Yan, K. Yue, X. Fan, X. Xu, J. Wang, M. Qin, Q. Zhang, X. Hou, X. Li and Y. Wang, Synthesis and bioactivity evaluation of ferrocene-based hydroxamic acids as selective histone deacetylase 6 inhibitors, *Eur. J. Med. Chem.*, 2023, **246**, 115004.

42 T. Stringer, L. Wiesner and G. S. Smith, Ferroquine-derived polyamines that target resistant Plasmodium falciparum, *Eur. J. Med. Chem.*, 2019, **179**, 78–83.

43 Y. Wang, P. Pigeon, W. Li, J. Yan, P. M. Dansette, M. Othman, M. J. McGlinchey and G. Jaouen, Diversity-oriented synthesis and bioactivity evaluation of N-substituted ferrocifen compounds as novel antiproliferative agents against TNBC cancer cells, *Eur. J. Med. Chem.*, 2022, **234**, 114202.

44 Y. Wang, P. Pigeon, S. Top, J. Sanz García, C. Troufflard, I. Ciofini, M. J. McGlinchey and G. Jaouen, Atypical Lone Pair–π Interaction with Quinone Methides in a Series of Imido-Ferrociphenol Anticancer Drug Candidates, *Angew. Chem., Int. Ed.*, 2019, **58**(25), 8421–8425.

45 Y. Wang, P. Pigeon, M. J. McGlinchey, S. Top and G. Jaouen, Synthesis and antiproliferative evaluation of novel hydroxypropyl-ferrociphenol derivatives, resulting from the modification of hydroxyl groups, *J. Organomet. Chem.*, 2017, **829**, 108–115.

46 H. Wang, X. Fan, P.-P. Xie, S. Yang, P. Pigeon, Y. Xiong, S. Gai, X. Qi, J. Wang, Q. Zhang, W. Li, H. Qian, M. J. McGlinchey, G. Jaouen, C. Zheng and Y. Wang, Deciphering the Diversified Metabolic Behavior of Hydroxyalkyl Ferrocidiphenols as Anticancer Complexes, *J. Med. Chem.*, 2024, **67**(2), 1209–1224.

47 H. Hagen, P. Marzenell, E. Jentzsch, F. Wenz, M. R. Veldwijk and A. Mokhir, Aminoferrocene-Based Prodrugs Activated by Reactive Oxygen Species, *J. Med. Chem.*, 2012, **55**(2), 924–934.

48 D.-W. Gao, Q. Gu and S.-L. You, An Enantioselective Oxidative C–H/C–H Cross-Coupling Reaction: Highly Efficient Method To Prepare Planar Chiral Ferrocenes, *J. Am. Chem. Soc.*, 2016, **138**(8), 2544–2547.

49 Z.-J. Cai, C.-X. Liu, Q. Gu, C. Zheng and S.-L. You, PdII-Catalyzed Regio- and Enantioselective Oxidative C−H/C−H Cross-Coupling Reaction between Ferrocenes and Azoles, *Angew. Chem., Int. Ed.*, 2019, **58**(7), 2149–2153.

50 C.-X. Liu, W.-W. Zhang, P. Yang, F. Zhao, Z. Feng, Q. Wang, S.-Z. Zhang, Q. Gu and S.-L. You, Pd-catalyzed asymmetric oxidative C-H/C-H cross-coupling reaction between dialkylaminomethylferrocenes and indolizines, *Chem Catal.*, 2022, **2**(1), 102–113.

51 P. Pigeon, Y. Wang, S. Top, F. Najlaoui, M. C. Garcia Alvarez, J. Bignon, M. J. McGlinchey and G. Jaouen, A New Series of Succinimido-ferrociphenols and Related Heterocyclic Species Induce Strong Antiproliferative Effects, Especially against Ovarian Cancer Cells Resistant to Cisplatin, *J. Med. Chem.*, 2017, **60**(20), 8358–8368.

52 H. Liu, F. Forouhar, A. J. Lin, Q. Wang, V. Polychronidou, R. K. Soni, X. Xia and B. R. Stockwell, Small-molecule allosteric inhibitors of GPX4, *Cell Chem. Biol.*, 2022, **29**(12), 1680–1693.

53 C. Xu, Z. Xiao, J. Wang, H. Lai, T. Zhang, Z. Guan, M. Xia, M. Chen, L. Ren, Y. He, Y. Gao and C. Zhao, Discovery of a Potent Glutathione Peroxidase 4 Inhibitor as a Selective Ferroptosis Inducer, *J. Med. Chem.*, 2021, **64**(18), 13312–13326.

54 J. K. Eaton, L. Furst, R. A. Ruberto, D. Moosmayer, A. Hilpmann, M. J. Ryan, K. Zimmermann, L. L. Cai, M. Niehues, V. Badock, A. Kramm, S. Chen, R. C. Hillig, P. A. Clemons, S. Gradl, C. Montagnon, K. E. Lazarski, S. Christian, B. Bajrami, R. Neuhaus, A. L. Eheim, V. S. Viswanathan and S. L. Schreiber, Selective covalent targeting of GPX4 using masked nitrile-oxide electrophiles, *Nat. Chem. Biol.*, 2020, **16**(5), 497–506.

55 D. Moosmayer, A. Hilpmann, J. Hoffmann, L. Schnirch, K. Zimmermann, V. Badock, L. Furst, J. K. Eaton, V. S. Viswanathan, S. L. Schreiber, S. Gradl and R. C. Hillig, Crystal structures of the selenoprotein glutathione peroxidase 4 in its apo form and in complex with the covalently bound inhibitor ML162, *Acta Crystallogr., Sect. D: Struct. Biol.*, 2021, **77**(Pt 2), 237–248.

56 Y. Wang, F. Heinemann, S. Top, A. Dazzi, C. Policar, L. Henry, F. Lambert, G. Jaouen, M. Salmain and A. Vessieres, Ferrocifens labelled with an infrared rhenium tricarbonyl tag: synthesis, antiproliferative activity, quantification and nano IR mapping in cancer cells, *Dalton Trans.*, 2018, **47**(29), 9824–9833.

57 L. Yin, J.-J. Duan, X.-W. Bian and S.-C. Yu, Triple-negative breast cancer molecular subtyping and treatment progress, *Breast Cancer Res.*, 2020, **22**(1), 61.

58 A. Borchert, J. Kalms, S. R. Roth, M. Rademacher, A. Schmidt, H. G. Holzhutter, H. Kuhn and P. Scheerer, Crystal structure and functional characterization of selenocysteine-containing glutathione peroxidase 4 suggests an alternative mechanism of peroxide reduction, *Biochim. Biophys. Acta, Mol. Cell Biol. Lipids*, 2018, **1863**(9), 1095–1107.